

Theoretical investigation on Friedel–Crafts reaction followed by rear-rangement/aromatization or ring-opening delivering benzoheterocycle and polycyclic alcohol, biaryl carboxylic acid

Nan Lu* and Chengxia Miao

College of Chemistry and Material Science, Shandong Agricultural University, Taian 271018, P. R. China.

***Corresponding Author:** Nan Lu, College of Chemistry and Material Science, Shandong Agricultural University, Taian 271018, P. R. China.

Received Date: September 16, 2024 | **Accepted Date:** September 30, 2024 | **Published Date:** October 10, 2024

Citation: Nan Lu and Chengxia Miao, (2024), Theoretical investigation on Friedel–Crafts reaction followed by rear-rangement/aromatization or ring-opening delivering benzoheterocycle and polycyclic alcohol, biaryl carboxylic acid, *International Journal of Clinical Case Reports and Reviews*, 19(2); DOI:10.31579/2690-4861/542

Copyright: © 2024, Nan Lu. This is an open-access article distributed under the terms of the Creative Commons Attribution License, which permits unrestricted use, distribution, and reproduction in any medium, provided the original author and source are credited.

Abstract:

Our DFT calculations provide the first theoretical investigation on CF₃SO₃H-promoted [1,5]Friedel–Crafts of 2-aryoxy-1,3-indandione and base-facilitated [1,6]Friedel–Crafts of 1,3-dicarbonyl. An intramolecular [1,5]Friedel–Crafts addition took place by activating carbonyl through H bridge with CF₃SO₃H. The resulting tertiary alcohol underwent dehydration producing reactive carbocation, which instigated a cascade of carboxyl group formation, ring-opening via C–C bond dissociation and C=C bond formation realizing aromatization. The product 3-aryl-2-benzo was yielded with recovered CF₃SO₃H. The electron-rich phenoxy group was deprotonated by HO- forming water. The initial nucleophilic addition to spatial-adjacent carbonyl afforded dieneone. It isomerized to the first product polycyclic alcohol. Then carboxylation occurred via hydroxyl shift followed by ring-opening aromatization to the second product biaryl carboxylic acid. The positive solvation effect is suggested by decreased absolute and activation energies in solution compared with in gas. These results are supported by Multiwfn analysis on FMO composition of specific TSs, and MBO value of vital bonding, breaking.

Key words: biaryl carboxylic acid; friedel–crafts; aromatization; ring-opening; benzoheterocycle

Introduction

As privileged structural components in biologically active compounds, the benzofuran and indole motifs are important in pharmaceutical science and drug industry due to versatile biological properties and chemical activities [1]. In this field, the benzofuran derivatives are especially significant as potential therapeutic agents. For instance, Shang researched the antioxidant activity of viniferifuran [2]. Song discovered aromatic polyketides from deep-sea cold-seep mussel associated endozooic fungus talaromyces minioluteus CS-138 [3]. Cao obtained cytotoxic alkaloids from micromelum integrerrimum [4]. However, traditional approaches often require multistep or complex reaction condition involving cascade reaction with α -imino Gold carbenes and Pd-catalyzed asymmetric Larock indole synthesis [5,6]. There fore the intramolecular C–N construction techniques offer efficient and sustainable routes [7,8] such as Wang's iron-catalyzed intramolecular C–H amination and He's Palladium-catalyzed enantioselective cacchi reaction for synthesis of N–H carbazoles and axially chiral 2,3-disubstituted indoles [9,10].

On the other, biaryl carboxylic acids are also key structural motifs in natural products for synthesis of axially chiral compounds. Biaryl lactone

was used for derivation of potential antimycotic agents against Candida strains [11]. In addition, binaphthyl scaffold like MeO-BINA-Cox is a class of versatile structure in asymmetric C–H functionalization [12]. Li prepared optically active 2,2'-Dibromo-6,6'-diido-1,1'-biphenyl as powerful precursor for modular synthesis of functionalized atropisomers [13]. Wei realized Fe-catalyzed difunctionalization of aryl titanates enabled by Fe/Ti synergism [14]. Linde developed atroposelective brominations to access chiral biaryl scaffolds applying high-valent Pd-catalysis [15]. Ansari utilized trichloromethyl carbanion in aqueous micelles to access carboxylic Acids from (Hetero)aryl halides [16]. Many efforts have been dedicated to these structures such as Palladium/norbornene-catalyzed decarbonylative difunctionalization of thioesters [17]. Despite with achievements of photoinduced protocol for aerobic oxidation of aldehydes to carboxylic acids, claisen approach to 4'-Ed4T and Palladium-catalyzed C–H ortho arylation of benzoic acids with diaryliodonium salt [18-20]. Some limitations still hampered owing to the requirement of prefunctionalization.

Tong found phosphine-catalyzed ($4 + 2$) annulations of δ -acetoxy allenotes and ketones to construct 1,3-cyclohexadienes [21]. Aspired by this, Liu developed [1,6]-type Friedel–Crafts reaction resulting in polycyclic alcohol then transformed into biaryl carboxylic acids through ring-opening rearrangement [22]. The 1,3-dicarbonyls were used to accomplish selective C–C bond formation previously [23,24]. One of the carbonyl groups is integrated into product structure. A recent progress was constrained [1,5]-type Friedel–Crafts reaction/rearrangement/aromatization process to synthesize 2-substituted-3-aryl benzofuran from easily available 2-aryoxy-1,3-indandione [25]. Although a range of benzoheterocycles were yielded, many problems still puzzled and there was no report about detailed mechanistic study explaining the promotion of $\text{CF}_3\text{SO}_3\text{H}$ as Bronsted acid (BA). How the reactive carbocation instigated cascade C–C bond dissociation and C=C bond formation? Why base was necessary for nucleophilic addition of electron-rich phenoxy group to spatial-adjacent carbonyl in generation of dieneone? What's specific process of ring-opening rearrangement and aromatization? To solve these questions in experiment, an in-depth theoretical study was necessary for this strategy also focusing on the comparison of [1,6]-, [1,5]-type Friedel–Crafts and excellent regio-, diastereoselectivity.

2 Computational details

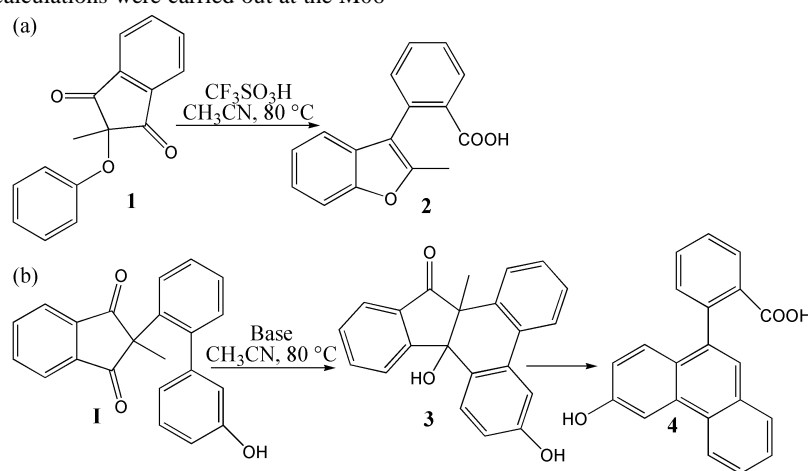
Optimized structures were obtained at M06-2X/6-31G(d) level of theory with GAUSSIAN09 [26]. In tests of popular DFT methods [27], M06-2X functional attained smaller standard deviation of difference between calculated value and experimental value in geometries than B3LYP including Becke's three-parameter hybrid functional combined with Lee–Yang–Parr correction for correlation [28,29]. The best compromise between accuracy and time consumption was provided with 6-31G(d) basis set on energy calculations. Also, M06-2X functional was found to give relatively accurate results for catalysed enantioselective ($4 + 3$), concerted [$4 + 2$], stepwise ($2 + 2$) cycloaddition and catalysed Diels–Alder reactions [30,31]. Together with the best performance on noncovalent interaction, M06-2X functional is believed to be suitable for this system [32–34]. The nature of each structure was verified by performing harmonic vibrational frequency calculations. Intrinsic reaction coordinate (IRC) calculations were examined to confirm the right connections among key transition-states and corresponding reactants and products. Harmonic frequency calculations were carried out at the M06-

2X/6-31G(d) level to gain zero-point vibrational energy (ZPVE) and thermodynamic corrections at 353 K and 1 atm for each structure in acetonitrile.

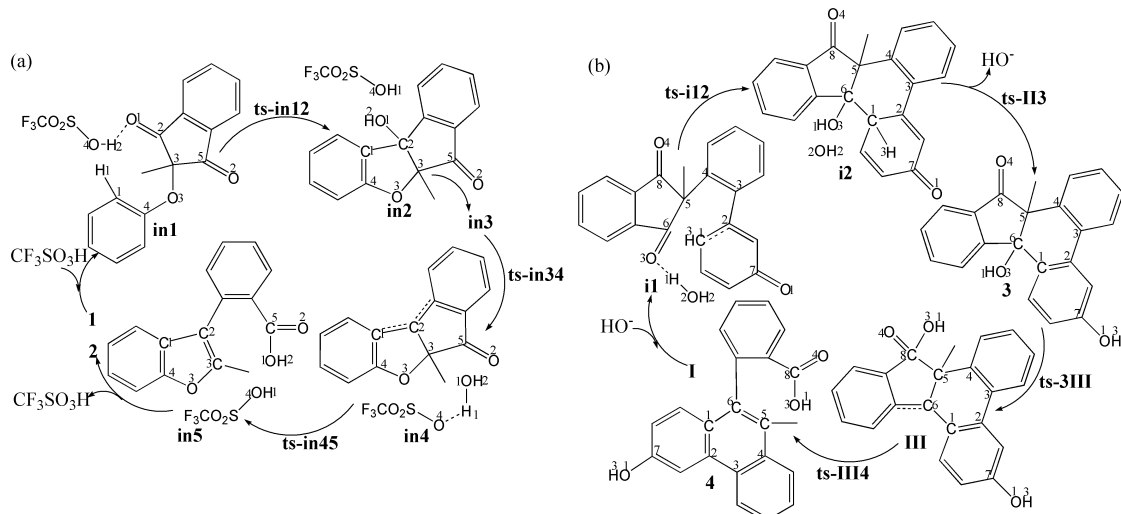
The solvation-corrected free energies were obtained at the M06-2X/6-311++G(d,p) level by using integral equation formalism polarizable continuum model (IEFPCM) in Truhlar's “density” solvation model [35–39] on the M06-2X/6-31G(d)-optimized geometries. As an efficient method obtaining bond and lone pair of a molecule from modern ab initio wave functions, NBO procedure was performed with Natural bond orbital (NBO3.1) to characterize electronic properties and bonding orbital interactions [40–42]. The wave function analysis was provided using Multiwfn_3.7_dev package [43] including research on frontier molecular orbital (FMO) and Mayer bond order (MBO).

3 Results and Discussion

The mechanism was explored for (a) $\text{CF}_3\text{SO}_3\text{H}$ -promoted [1,5] Friedel–Crafts of 2-aryoxy-1,3-indandione **1** leading to 2-substituted-3-aryl benzofuran **2**; (b) Base-facilitated [1,6]Friedel–Crafts of 1,3-dicarbonyl **I** resulting in polycyclic alcohol **3** then transformed into biaryl carboxylic acid **4** (Scheme 1). Illustrated by black arrow of Scheme 2a, an intramolecular [1,5]Friedel–Crafts addition of 1,3-indandione **1** took place by activating carbonyl through H bridge with $\text{CF}_3\text{SO}_3\text{H}$ as Bronsted acid. Then the resulting tertiary alcohol **in3** underwent dehydration assisted by $\text{CF}_3\text{SO}_3\text{H}$ to produce reactive carbocation **in4**, which then instigated a cascade of carboxyl group formation, ring-opening via C–C bond dissociation and C=C bond formation realizing aromatization. The final product 3-aryl-2-benzo **2** was yielded binding recovered $\text{CF}_3\text{SO}_3\text{H}$. Shown by black arrow of Scheme 2b, the electron-rich phenoxy group was deprotonated under the catalysis of base HO^- forming water. The initial nucleophilic addition underwent with spatial-adjacent carbonyl resulting in dieneone **II** after removal of HO^- . Subsequently, **II** isomerized to the first product polycyclic alcohol **3**, from which carboxylation proceeds via hydroxyl shift rearrangement followed by ring-opening aromatization leading to the second product biaryl carboxylic acid **4**. The schematic structures of optimized TSs in Scheme 2 were listed by Figure 1. The activation energy was shown in Table 1 for all steps. Supplementary Table S1, Table S2 provided the relative energies of all stationary points. According to experiment, the Gibbs free energies in acetonitrile solution phase are discussed here.



Scheme 1 (a) $\text{CF}_3\text{SO}_3\text{H}$ -promoted [1,5] Friedel–Crafts of 2-aryoxy-1,3-indandione **1** leading to 2-substituted-3-aryl benzofuran **2**; (b) Base-facilitated [1,6] Friedel–Crafts of 1,3-dicarbonyl **I** resulting in polycyclic alcohol **3** then transformed into biaryl carboxylic acid **4**.

**Scheme 2:** Proposed reaction mechanism of TS is named according to the two intermediates it connects.

Species	ΔG_{gas}	$\Delta G_{\text{sol(CH3CN)}}$
1	0.00	0.00
2	-25.36	-29.57
1+CF₃SO₃H	0.00	0.00
in1	-16.53	-4.90
ts-in12	13.57	11.25
in2	-28.20	-16.00
in3	-1.71	7.71
ts-in34	19.91	14.22
in4	6.93	-0.52
ts-in45	13.12	0.54
in5	-39.98	-31.98
Species	ΔG_{gas}	$\Delta G_{\text{sol(CH3CN)}}$
I+OH	0.00	0.00
i1	-58.08	-10.32
ts-i12	-48.44	-1.15
i2	-62.84	-14.39
I	0.00	0.00
II	11.20	1.36
ts-II3	44.52	30.43
3	-2.96	-9.64
ts-3III	22.10	11.65
III	8.95	3.38
ts-III4	21.23	13.19
4	-20.81	-26.93

Table S1. Calculated relative energies (all in kcal mol⁻¹, relative to isolated species) for the ZPE-corrected Gibbs free energies (ΔG_{gas}), Gibbs free energies for all species in solution phase (ΔG_{sol}) at 353 K by M06-2X/6-311++G(d,p)//M06-2X/6-31G(d) method and difference between absolute energy.

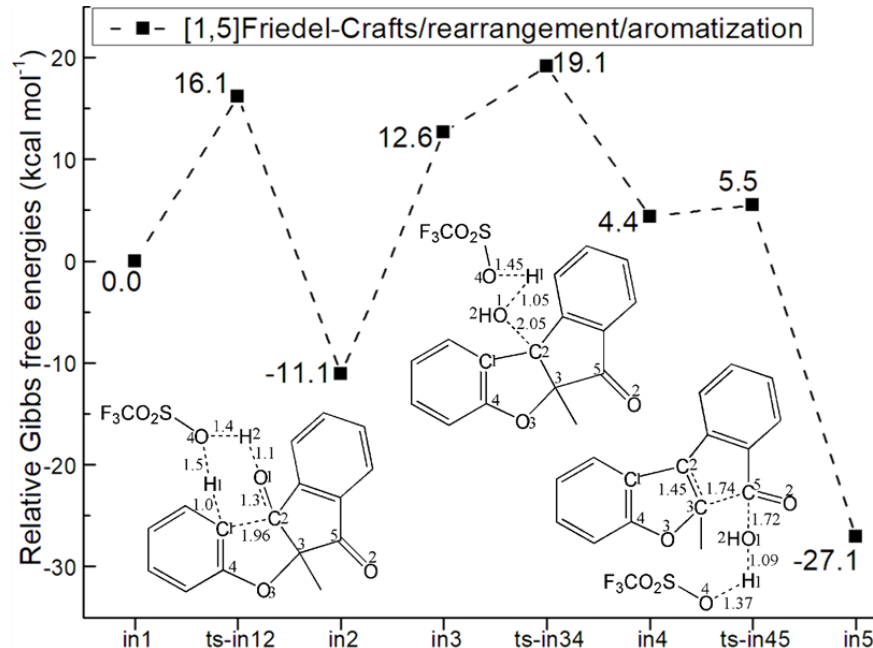
TS	$\Delta G^{\ddagger}_{\text{gas}}$	$\Delta G^{\ddagger}_{\text{sol}}$
ts-in12 (360i)	30.1	16.1
ts-in34 (292i)	21.6	6.5
ts-in45 (243i)	6.2	1.1
ts-i12 (248i)	9.6	9.2
ts-II3 (1812i)	33.3	29.1
ts-3III (377i)	25.1	21.3
ts-III4 (100i)	12.3	9.8

Table S2. The activation energy (local barrier) (in kcal mol⁻¹) of all reactions in the gas, solution phase calculated with M06-2X/6-311++G(d,p)//M06-2X/6-31G(d) method.

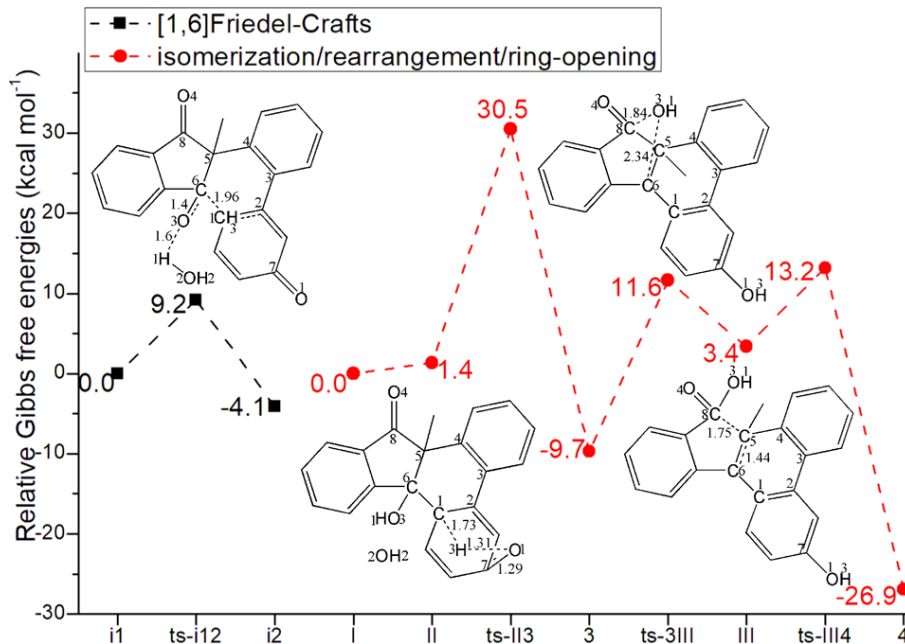
TS	$\Delta G^\ddagger_{\text{gas}}$	$\Delta G^\ddagger_{\text{sol}}$
ts-in12	30.1	16.2
ts-in34	21.6	6.5
ts-in45	6.2	1.1
ts-i12	9.6	9.2
ts-II3	33.3	29.1
ts-III	25.1	21.3
ts-III4	12.3	9.8

Table 1 The activation energy (in kcal mol⁻¹) of all reactions in gas and solvent

(a)



(b)

**Figure 1:** Relative Gibbs free energy profile in solvent phase starting from complex (a) in1 (b) i1, I (Bond lengths of optimized TSs in Å).

3.1 [1,5] Friedel-Crafts/rearrangement/aromatization

The initial complex is located as **in1** involving H bond stabilization between $\text{CF}_3\text{SO}_3\text{H}$ and carbonyl of **I**. An intramolecular [1,5]Friedel–Crafts addition took place via **ts-in12** in step 1 with the activation energy of 16.1 kcal mol⁻¹ relative to starting point **in1** exothermic by -11.1 kcal mol⁻¹ producing tertiary alcohol **in2** (black dash line of Figure 1a). The transition vector includes dual proton transfer $\text{C1}\cdots\text{H1}\cdots\text{O4}, \text{O4}\cdots\text{H2}\cdots\text{O1}$, resultant stretching of C2-O1 double bond to single one and the slightly delayed nucleophilic addition of C1 to C2 (1.0, 1.5, 1.4, 1.1, 1.3, 1.96 Å) (Figure S1a). Obviously, the driving force is attributed by H bridge from $\text{CF}_3\text{SO}_3\text{H}$ via simultaneously activating nucleophilic C1 and carbonyl C2=O1. Once C1-C2 is bonded, carbonyl becomes hydroxyl O1H2 in the new five membered ring of **in2**, which transformed to **in3** more reactive with relative energy increased by 23.7 kcal mol⁻¹ ready to initiate next step.

Then assisted by $\text{CF}_3\text{SO}_3\text{H}$, the resulting tertiary alcohol **in3** undergoes dehydration via **ts-in34** as step 2 with activation energy of 6.5 kcal mol⁻¹ endothermic by 4.4 kcal mol⁻¹ producing reactive carbocation **in4**. The transition vector suggests that the obtained proton H1 from C1 in previous step 1 is handed over to hydroxyl O1H2 by O4 of $\text{CF}_3\text{SO}_3\text{H}$ to assemble water molecule H1-O1H2. This causes the breaking of C2-O1 single bond concertedly (1.45, 1.05, 2.05 Å) (Figure S1b). The leaving of O1H2 from C2 makes it positive and sp² hybrid in carbocation **in4**, where there is still O4···H1O1 H bonding.

At last, a cascade rearrangement/aromatization takes place via **ts-in45** in subsequent step 3 with low activation energy of 1.1 kcal mol⁻¹ affording **in5** exothermic by -27.1 kcal mol⁻¹. The transition vector is complicated contains a series of atomic motion. On one hand, the water returns H1 to O4 of CF_3SO_3 facilitating its recovery via O1···H1···O4 (1.09, 1.37 Å). The hydroxyl O1H2 is thus approaching another carbonyl C5=O2 via O1···C5 (1.72 Å) forming carboxyl group. On the other, C3-C5 bond is dissociated inducing ring-opening and C2=C3 double bond formation realizing aromatization (1.74, 1.45 Å) (Figure S1c). The final **in5** is rather stable combining recovered $\text{CF}_3\text{SO}_3\text{H}$ and product 3-aryl benzofuran involving carboxyl moiety. Ultimately, the [1,5]Friedel–Crafts in step 1 is determined to be rate-limiting for $\text{CF}_3\text{SO}_3\text{H}$ -promoted whole process.

3.2 [1,6] Friedel–Crafts/isomerization/carboxylation/ring-opening aromatization

As a comparison, [1,6]Friedel–Crafts was also explored from 1,3-dicarbonyl **I** facilitated by base HO⁻ (black dash line of Figure 1b). In

initial **i1**, the electron-rich phenoxy group was deprotonated by additional HO⁻ forming water H1-O2H2, which activated spatial-adjacent carbonyl via H bonding. Therefore, the nucleophilic addition from C1 to C6 occurs readily via **ts-i12** in step 1 with activation energy of 9.2 kcal mol⁻¹ exothermic by -4.1 kcal mol⁻¹ resulting in **i2** delivering dieneone intermediate **II** after removal of HO⁻. The transition vector corresponds to the approaching of H1 to O3, elongation of carbonyl C6-O3 from double bond to single and C1-C6 linkage (1.6, 1.4, 1.96 Å) (Figure S1d). The typical C1-C6 bond gives new six membered ring in stable **i2**.

Without HO⁻, **II** turns to be more reactive with higher relative energy (1.4 kcal mol⁻¹) than **I**. Subsequently, the isomerization of **II** in step 2 happens via **ts-II3** with activation energy of 29.1 kcal mol⁻¹ exothermic by -9.7 kcal mol⁻¹ generating **3** (red dash line of Figure 1b). The transition vector reveals detailed atomic motion comprising proton H3 transfer from C1 to O1 and the resultant stretching of carbonyl C7-O1 from double to single (1.73, 1.31, 1.29 Å) (Figure S1e). As the first product polycyclic alcohol, **3** involves the recovered phenolic hydroxyl group O1H3.

In next step 3, the rearrangement via hydroxyl shift proceeds via **ts-3III** with activation energy of 21.3 kcal mol⁻¹ yielding cation **III** stabilized by two conjugated phenyl ring endothermic by 3.4 kcal mol⁻¹. This process is illustrated according to the transition vector composed of hydroxyl O3H1 leaving from C6 to C8 that is C6···O3 breaking and C8···O3 bonding (2.34, 1.84 Å) (Figure S1f). The outcome not only includes formation of reactive cation at C6 but carboxylation producing new carboxyl group O4=C8-O3H1.

From reactive **III**, the final ring-opening aromatization is easy to be initiated via **ts-III4** in step 4 with a low barrier of only 9.8 kcal mol⁻¹ exothermic by -26.9 kcal mol⁻¹ affording **4** as the second product biaryl carboxylic acid. This step is quite favorable both from kinetics and thermodynamics. Demonstrated by the transition vector, the ring-opening is accomplished via C5···C8 cleavage and aromatization through C5-C6 shortened from single bond to double (1.75, 1.44 Å) (Figure S1g). Comparatively, the isomerization of dieneone in step 2 is determined to be rate-limiting for base-facilitated [1,6]Friedel–Crafts case.

To highlight the idea of feasibility for changes in electron density and not molecular orbital interactions are responsible of the reactivity of organic molecules, quantum chemical tool Multiwfns was applied to analyze of electron density such as MBO results of bonding atoms and contribution of atomic orbital to HOMO of typical TSs (Table S3, Figure S2). These results all confirm the above analysis.

	O4···H2	H2···O1	C1···C2	C2···O1	
ts-in12	0.23	0.45	0.45	1.29	
	O4···H1	H1···O1	C2···O1		
ts-in34	0.22	0.48	0.28		
	O1···H1	H1···O4	O1···C5	C5···C3	C3···C2
ts-in45	0.43	0.25	0.45	0.64	1.27
	H1···O3	C6···O3	C1···C6		
ts-i12	0.17	1.37	0.50		
	C1···H3	H3···O1	C7···O1		
ts-II3	0.39	0.39	1.34		
	C6···O3	C8···O3			
ts-3III	0.23	0.43			
	C5···C8	C5···C6			
ts-III4	1.24	0.51			

Table S3. Mayer bond order (MBO) of typical TSs

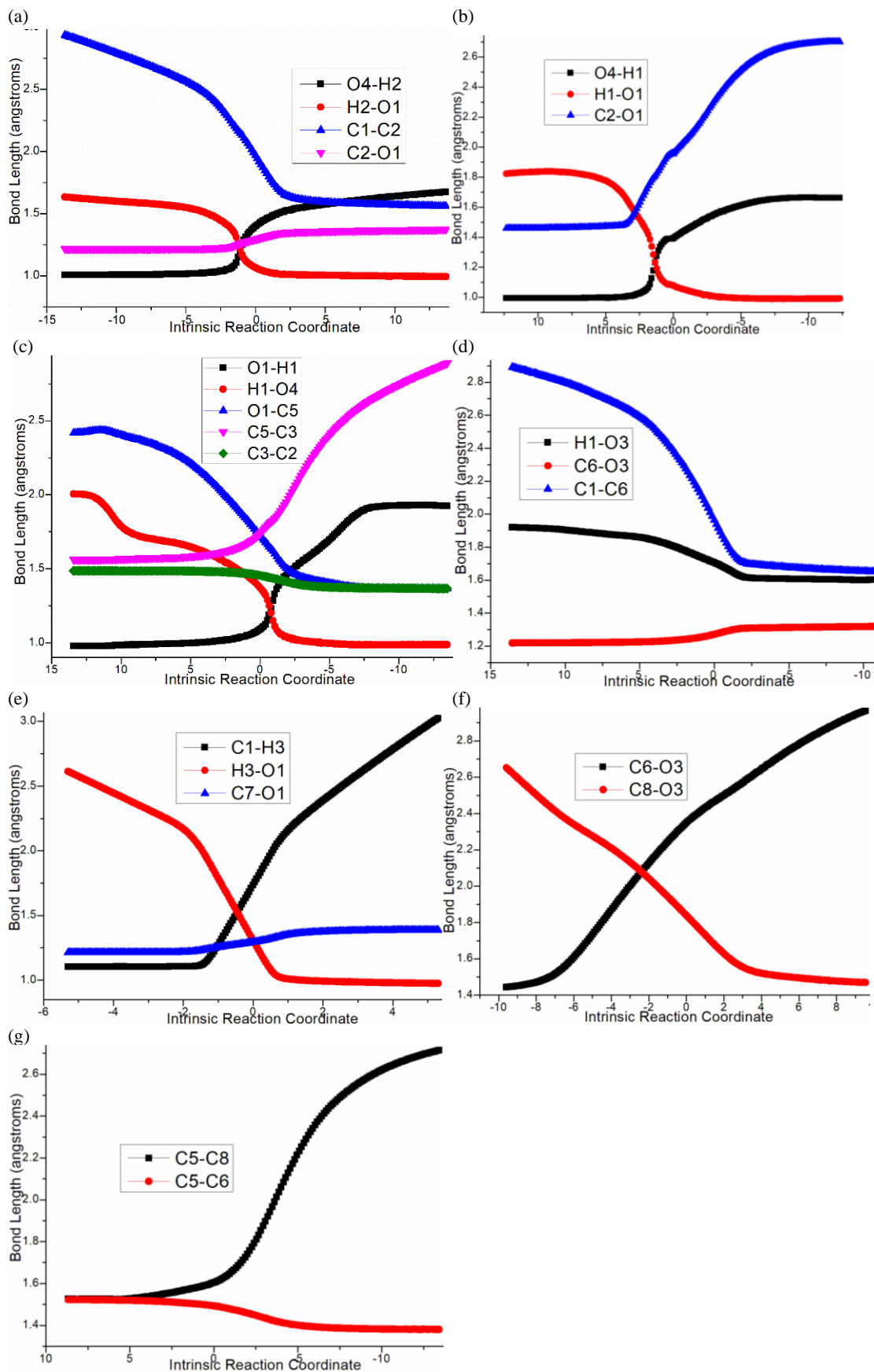


Figure S1. Evolution of bond lengths along the IRC for (a) ts-in12 (b) ts-in34 (c) ts-in45 (d) ts-i12 (e) ts-II3 (f) ts-3III (g) ts-III4 at M06-2X/6-311++G(d,p) level.

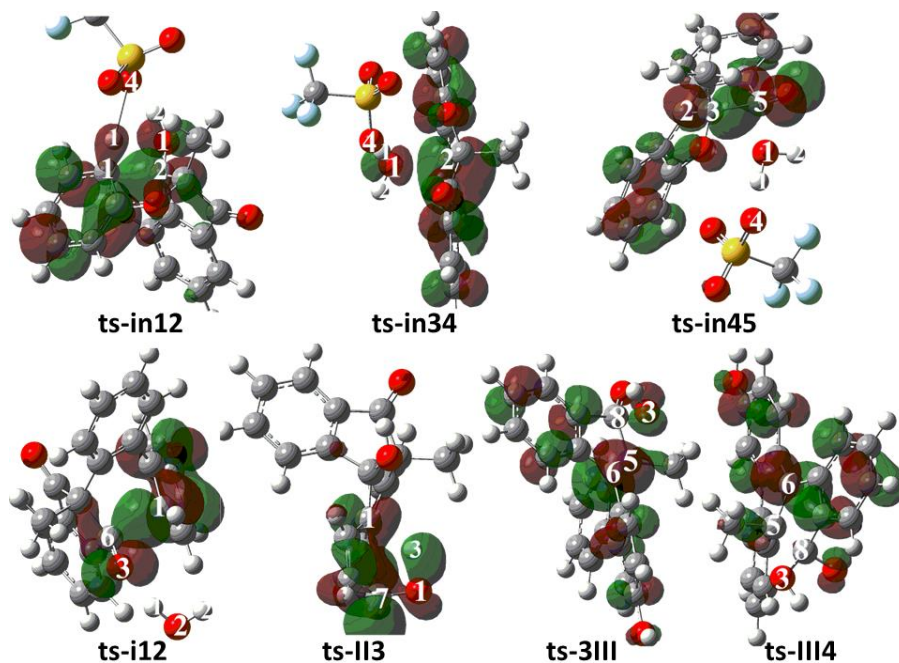


Figure S2. Highest Occupied Molecular Orbital (HOMO) of typical TSs. Different colors are used to identify the phase of the wave functions.

4 Conclusions

Our DFT calculations provide the first theoretical investigation on $\text{CF}_3\text{SO}_3\text{H}$ -promoted [1,5]Friedel–Crafts of 2-aryoxy-1,3-indandione leading to 2-substituted-3-aryl benzofuran and base-facilitated [1,6]Friedel–Crafts of 1,3-dicarbonyl resulting in polycyclic alcohol then transformed into biaryl carboxylic acid. For the former, an intramolecular [1,5]Friedel–Crafts addition of 1,3-indandione took place by activating carbonyl through H bridge with $\text{CF}_3\text{SO}_3\text{H}$. The resulting tertiary alcohol underwent dehydration assisted by $\text{CF}_3\text{SO}_3\text{H}$ producing reactive carbocation, which then instigated a cascade of carboxyl group formation, ring-opening via C–C bond dissociation and C=C bond formation realizing aromatization. The final product 3-aryl-2-benzo was yielded binding recovered $\text{CF}_3\text{SO}_3\text{H}$. For the latter, the electron-rich phenoxy group was deprotonated under the catalysis of HO^- forming water. The initial nucleophilic addition underwent with spatial-adjacent carbonyl affording dieneone after removal of HO^- . Subsequently, dieneone isomerized to the first product polycyclic alcohol, from which carboxylation proceeds via hydroxyl shift rearrangement followed by ring-opening aromatization leading to the second product biaryl carboxylic acid. Comparatively, [1,5]Friedel–Crafts in step 1 is determined to be rate-limiting for $\text{CF}_3\text{SO}_3\text{H}$ -prompted process. While the isomerization of dieneone in step 2 is rate-limiting for base-facilitated [1,6]Friedel–Crafts case. The positive solvation effect is suggested by decreased absolute and activation energies in acetonitrile solution compared with in gas. These results are supported by Multiwfns analysis on FMO composition of specific TSs, and MBO value of vital bonding, breaking.

Electronic Supplementary Material

Supplementary data available: [Computation information and cartesian coordinates of stationary points; Calculated relative energies for the ZPE-corrected Gibbs free energies (ΔG_{gas}), and Gibbs free energies (ΔG_{sol}) for all species in solution phase at 353 K.]

Author contributions: Conceptualization, Nan Lu; Methodology, Nan Lu; Software, Nan Lu; Validation, Nan Lu; Formal Analysis, Nan Lu; Investigation, Nan Lu; Resources, Nan Lu; Data Curation, Nan Lu; Writing-Original Draft Preparation, Nan Lu; Writing-Review & Editing, Nan Lu; Visualization, Nan Lu; Supervision, Chengxia Miao; Project Administration, Chengxia Miao; Funding Acquisition, Chengxia Miao. All authors have read and agreed to the published version of the manuscript.

Funding: This work was supported by National Natural Science Foundation of China (21972079) and Key Laboratory of Agricultural Film Application of Ministry of Agriculture and Rural Affairs, P.R. China.

Conflict of interest: The authors declare no conflict of interest.

References

- Heravi, M. M.; M Zadirsjan, V. (2015). Recent Advances in the Synthesis of Benzo[b]furans. In *Advances in Heterocyclic Chemistry*, 117, 261–376.
- Shang, Y.; Zhou, H.; Li, X.; Zhou, J.; Chen, K. (2019). Theoretical studies on the antioxidant activity of viniferifuran. *New J. Chem.* 43, 15736–15742.
- Song, Q.; Yang, S. Q.; Li, X. M.; Hu, X. Y.; Li, X. et al. (2022). Aromatic Polyketides from the Deep-Sea Cold-Deep Mussel Asso-ciated Endozoic Fungus *Talaromyces minioluteus* CS-138. *Mar. Drugs.* 20, 529–538.
- Cao, N. K.; Chen, Y. M.; Jiang, Y.; Li, J.; Tu, P. F. et al. (2020). Isolation and structure characterization of cytotoxic alkaloids from *Micromelum integerrimum*. *Phytochemistry*, 178, No. 112463.
- Sun, Q.; Hübler, C.; Kahle, J.; Mackenroth, A. V.; Rudolph, M. et al. (2024). Cascade Reactions of Ar-yl-Substituted Terminal Alkynes Involving in Situ-Generated α -Imino Gold Carbenes. *Angew. Chem. Int. Ed.* 63, No. e2023137.

6. Zhang, G.; Yang, B.; Yang, J.; Zhang, J. (2024). Pd-Catalyzed Asymmetric Larock Indole Synthesis to Access Axially Chiral N-Arylindoles. *J. Am. Chem. Soc.* 146, 5493–5501.
7. Xie, F.; Sun, Y.; Song, H.; Zhao, J.; Zhang, Z. et al. (2021). Cascade Reaction of 2-Naphthols and Azirines: One-Pot Synthesis of C-3 Naphthol-Substituted Benzo[e]indoles. *J. Org. Chem.* 86, 15631–15639.
8. Mao, J.; Wang, Z.; Xu, X.; Liu, G.; Jiang, R. et al. (2019). Synthesis of Indoles through Domino Reactions of 2-Fluorotoluenes and Nitriles. *Angew. Chem., Int. Ed.* 58, 11033–11038.
9. Wang, Z. L.; Zhang, Y. H.; Huang, J. Y.; Zhou, J.; Yu, Y. Q. et al. (2023). Iron-catalyzed intramolecular C–H amination for the synthesis of N–H carbazoles and indoles. *Green Chem.* 25, 4463–4468.
10. He, Y. P.; Wu, Hu.; Wang, Q.; Zhu, J. (2020). Palladium-Catalyzed Enantioselective Cacchi Reaction: Asymmetric Synthesis of Axially Chiral 2,3-Disubstituted Indoles. *Angew. Chem., Int. Ed.* 59, 2105–2109.
11. Chao, M.; Wang, F.; Xu, L. L.; Ju, Y. P.; Chen, Z. X. et al. (2021). Cerium Ammonium Nitrate-Mediated Access to Biaryl Lactones: Substrate Scopes and Mechanism Studies. *J. Org. Chem.* 86, 13371–13380.
12. Yue, Q.; Liu, B.; Liao, G.; Shi, B. F. (2022). Binaphthyl Scaffold: A Class of Versatile Structure in Asymmetric C–H Functionalization. *ACS Catal.* 12, 9359–9396.
13. Li, Y. Y.; Duan, L. H.; Hong, B. Q.; Gu, Z. H. (2023). Preparation of Optically Active 2,2'-Dibromo-6,6'-diiodo-1,1'-biphenyl: A Powerful Precursor for Modular Synthesis of Functionalized Atropisomers. *Chin. J. Chem.* 41, 3515–3520.
14. Wei, Y. M.; Ma, X. D.; Wang, M. F.; Duan, X. F. (2023). Fe-Catalyzed Difunctionalization of Aryl Titanates Enabled by Fe/Ti Synergism. *Org. Lett.* 25, 2745–2749.
15. Linde, S. T.; Corti, V.; Lauridsen, V. H.; Lamhauge, J. N.; Jørgensen, K. A. et al. (2023). Atroposelective brominations to access chiral biaryl scaffolds using high-valent Pd-catalysis. *Chem. Sci.* 14, 3676–3681.
16. Ansari, T. N.; Sharma, S.; Hazra, S.; Hicks, F.; Leahy, D. K. et al. (2022). Trichloromethyl Carbanion in Aqueous Micelles: Mechanistic Insights and Access to Carboxylic Acids from (Hetero)aryl Halides. *ACS Catal.* 12, 15686–15695.
17. Han, M. L.; Chen, J. J.; Xu, H.; Huang, Z. C.; Huang, W. et al. (2021). Palladi-um/Norbornene-Catalyzed Decarbonylative Difunctionalization of Thioesters. *JACS Au*, 1, 1877–1884.
18. Xu, J.; Yue, X. G.; He, L.; Shen, J.; Ouyang, Y. et al. (2022). Photoinduced Protocol for Aerobic Oxidation of Aldehydes to Carboxylic Acids under Mild Conditions. *ACS Sustain*, 10, 14119–14125.
19. Gallagher, W. P.; Deshpande, P. P.; Li, J.; Katipally, K.; Sausker, J. (2015). A Claisen Approach to 4'-Ed4T. *J. Org. Lett.* 17, 14–17.
20. (a) Wu, Z. Q.; Chen, S.; Hu, C. X.; Li, Z. K.; Xiang, H. F. et al. (2013). Palladium-Catalyzed C H ortho Arylation of Benzoic Acids with Diaryliodonium Salts in Water. *ChemCatChem*, 5, 2839–2842.
21. Zhang, Y. W.; Tong, X. F. (2017). Construction of Complex 1,3-Cyclohexadienes via Phosphine-Catalyzed (4 + 2) Annulations of δ-Acetoxy Allenoates and Ketones. *Org. Lett.* 19, 5462–5465.
22. Liu, S.; Cheng, L.; Liu, L. (2004). Synthesis of Biaryl Carboxylic Acids through a Cascade Suzuki–Miyaura Coupling/Friedel–Crafts Alkyl-ation/Lewis-Acid-
23. Catalyzed Rearrangement/Aromatization Process. *Org. Lett.* 26, 1902–1907.
24. Liu, Q.; Liu, J. J.; Cheng, L.; Wang, D.; Liu, L. (2018). TEMPO promoted direct multi-functionalization of terminal alkynes with 2-oxindoles/benzofuran-2(3H)-one. *Org. Biomol. Chem.* 16, 5228–5231.
25. Huang, H. Y.; Cheng, L.; Liu, J. J.; Wang, D.; Liu, L. et al. (2017). Transition-Metal-Free Alkylation of 2-Oxindoles through Radi-cal–Radical Coupling. *J. Org. Chem.* 82, 2656–2663.
26. Liu, S.; Liu, Q.; Cheng, L.; Liu, L. (2024). Construction of 2-Substituted-3-aryl Benzofurans and Indoles through an Acid-Catalyzed Cascade Intramolecular Friedel–Crafts Reaction/Rearrangement/Aromatization Process. *J. Org. Chem.* 89, 11716–11726.
27. Frisch, M. J.; Trucks, G. W.; Schlegel, H. B. et al. (2010). Gaussian 09 (Revision B.01), Gaussian, Inc., Wallingford, CT.
28. Stephens, P. J.; Devlin, F. J.; Chabalowski, C. F.; Frisch, M. J. (1994). Ab initio Calculation of Vibrational Absorption and Circular Di-choroism Spectra Using Density Functional Force Fields, *J. Phys. Chem.* 98, 11623–11627.
29. Becke, A. D. (1996). Density-functional thermochemistry. IV. A new dynamical correlation functional and implications for exact-exchange mixing. *J. Chem. Phys.* 104, 1040–1046.
30. Lee, C. T.; Yang, W. T.; Parr, R. G. (1998). Development of the Colle-Salvetti correlation-energy formula into a functional of the electron density. *Phys. Rev. B*, 37, 785–789.
31. Li, X.; Kong, X.; Yang, S.; Meng, M.; Zhan, X. et al. (2019). Bifunctional Thiourea-Catalyzed Asymmetric Inverse-Electron-Demand Diels-Alder Reaction of Allyl Ketones and Vinyl 1,2-Diketones via Dienolate Intermediate, *Org. Lett.* 21, 1979–1983.
32. Krenske, E. H.; Houk, K. N.; Harmata, M. (2015). Computational Analysis of the Stereochemical Outcome in the Imidazolidinone-Catalyzed Enantioselective (4 + 3)-Cycloaddition Reaction, *J. Org. Chem.* 80, 744–750.
33. Lv, H.; Han, F.; Wang, N.; Lu, N.; Song, Z. et al. (2022). Ionic Liquid Catalyzed C–C Bond Formation for the Synthesis of Polysubstituted Olefins. *Eur. J. Org. Chem.* e202201222.
34. Zhuang, H.; Lu, N.; Ji, N.; Han, F.; Miao, C. (2021). Bu4NHSO4-Catalyzed Direct N-Allylation of Pyrazole and its Derivatives with Allylic Alcohols in Water: A Metal-free, Recyclable and Sustainable System. *Advanced Synthesis & Catalysis*, 363, 5461–5472.
35. Lu, N.; Liang, H.; Qian, P.; Lan, X.; Miao, C. (2020). Theoretical investigation on the mechanism and enantioselectivity of organocatalytic asymmetric Povarov reactions of anilines and aldehydes. *Int. J. Quantum Chem.* 120, e26574.
36. Tapia, O. (1992). Solvent effect theories: Quantum and classical formalisms and their applications in chemistry and biochemistry. *J. Math. Chem.* 10, 139–181.
37. Tomasi, J.; Persico, M. (1994). Molecular Interactions in Solution: An Overview of Methods Based on Continuous Distributions of the Solvent. *Chem. Rev.* 94, 2027–2094.
38. Simkin, B. Y.; Sheikhet, I. (1995). Quantum Chemical and Statistical Theory of Solutions—A Computational Approach, Ellis Horwood, London .
39. Tomasi, J.; Mennucci, B.; Cammi, R. (2005). Quantum Mechanical Continuum Solvation Models. *Chem. Rev.*, 105, 2999–3093.

39. Marenich, A. V.; Cramer, C. J.; Truhlar, D. G. (2009). Universal Solvation Model Based on Solute Electron Density and on a Continuum Model of the Solvent Defined by the Bulk Dielectric Constant and Atomic Surface Tensions. *J. Phys. Chem. B*, 113, 6378–6396.
40. Reed, A. E.; Weinstock, R. B.; Weinhold, F. (1985). Natural population analysis. *J. Chem. Phys.* 83, 735-746.
41. Reed, A. E.; Curtiss, L. A.; Weinhold, F. (1988). Intermolecular interactions from a natural bond orbital donor-acceptor view point. *Chem. Rev.* 88, 899-926.
42. Foresman, J. B.; Frisch, A. (1996). Exploring Chemistry with Electronic Structure Methods, 2nd ed., Gaussian, Inc., Pittsburgh.
43. Lu, T.; Chen, F. (2012). Multiwfn: A multifunctional wavefunction analyzer. *J. Comput. Chem.* 33, 580-592.



This work is licensed under Creative Commons Attribution 4.0 License

To Submit Your Article Click Here:

[Submit Manuscript](#)

DOI:[10.31579/2690-4861/542](https://doi.org/10.31579/2690-4861/542)

Ready to submit your research? Choose Auctores and benefit from:

- fast, convenient online submission
- rigorous peer review by experienced research in your field
- rapid publication on acceptance
- authors retain copyrights
- unique DOI for all articles
- immediate, unrestricted online access

At Auctores, research is always in progress.

Learn more <https://auctoresonline.org/journals/international-journal-of-clinical-case-reports-and-reviews>

Software: GAUSSIAN09

Level of Theory: M06-2X

Basis Set: 6-31G(d)

Geometry [Cartesian coordinates]:

Optimized Cartesian coordinates for ts-in12

Center Number	Atomic Number	Atomic Type	Coordinates (Angstroms)		
			X	Y	Z
1	6	0	2.109828	0.975638	-0.366288
2	6	0	1.832608	0.448304	-1.728663
3	6	0	0.503797	0.031928	-1.823048
4	6	0	-0.217261	0.334465	-0.548292
5	8	0	-1.216647	1.144291	-0.685831
6	8	0	3.074779	1.578939	0.018778
7	6	0	2.685316	0.388854	-2.826607
8	6	0	2.178787	-0.121270	-4.016650
9	6	0	0.844070	-0.539377	-4.108675
10	6	0	-0.014883	-0.454584	-3.016467
11	1	0	3.710212	0.735565	-2.739536
12	1	0	2.818715	-0.189376	-4.890582
13	1	0	0.472296	-0.924110	-5.053085
14	1	0	-1.055931	-0.754167	-3.087312
15	6	0	0.914643	0.523741	0.522945
16	8	0	1.346749	-0.816853	0.878026
17	6	0	0.626866	1.379140	1.722096
18	1	0	0.011825	0.846217	2.451158
19	1	0	1.577758	1.654448	2.186602
20	1	0	0.107685	2.295126	1.424888
21	6	0	0.458095	-1.738439	0.484949
22	6	0	-0.876479	-1.301945	0.324395
23	6	0	0.882216	-2.992527	0.047191
24	6	0	-1.785696	-2.138827	-0.381440
25	1	0	-1.301223	-0.668839	1.109675
26	6	0	-0.034959	-3.773348	-0.636210
27	1	0	1.916011	-3.291207	0.176320
28	6	0	-1.359541	-3.345074	-0.883476
29	1	0	-2.815877	-1.807879	-0.476008
30	1	0	0.288361	-4.734113	-1.026609
31	1	0	-2.036089	-3.989890	-1.433170
32	16	0	-2.762380	1.102010	2.525050
33	8	0	-2.295550	2.407146	2.963550
34	8	0	-2.092102	-0.079186	3.076244
35	8	0	-2.932493	0.988967	1.027758
36	1	0	-1.871597	1.221544	0.151826
37	6	0	-4.505964	0.968206	3.072395
38	9	0	-5.029843	-0.182345	2.658960
39	9	0	-4.558595	1.013046	4.398456
40	9	0	-5.220302	1.969968	2.575734

Optimized Cartesian coordinates for ts-in34

Center Number	Atomic Number	Atomic Type	Coordinates (Angstroms)		
			X	Y	Z

1	6	0	1.104241	-1.676375	0.950820
2	6	0	2.435602	-1.803904	0.239666
3	6	0	2.928823	-0.538315	-0.140125
4	6	0	1.893435	0.433139	0.217312
5	8	0	0.638229	-0.110040	-1.310060
6	8	0	0.371637	-2.559036	1.282025
7	6	0	3.159542	-2.956522	-0.001317
8	6	0	4.398697	-2.828115	-0.637028
9	6	0	4.890554	-1.575796	-1.010372
10	6	0	4.157569	-0.410701	-0.772791
11	1	0	2.763971	-3.923271	0.294954
12	1	0	4.988022	-3.714536	-0.848913
13	1	0	5.856746	-1.506471	-1.499419
14	1	0	4.541025	0.559561	-1.071016
15	6	0	1.066688	-0.170797	1.311914
16	8	0	-0.100645	0.635303	1.353390
17	6	0	1.741240	-0.054596	2.693813
18	1	0	1.918692	0.997150	2.931284
19	1	0	1.047048	-0.480010	3.422275
20	1	0	2.685710	-0.601419	2.734928
21	6	0	0.267428	1.825025	0.824303
22	6	0	1.529673	1.801517	0.179299
23	6	0	-0.512334	2.976905	0.873241
24	6	0	2.025211	2.951800	-0.461000
25	1	0	-0.332616	-0.393804	-1.028056
26	6	0	0.018349	4.101639	0.268038
27	1	0	-1.497268	2.952244	1.321140
28	6	0	1.273041	4.102464	-0.386092
29	1	0	2.974601	2.929704	-0.985465
30	1	0	-0.560446	5.019989	0.280344
31	1	0	1.628767	5.016815	-0.847718
32	16	0	-2.670943	-0.131604	-0.189588
33	8	0	-2.364287	1.275105	-0.462048
34	8	0	-3.265278	-0.457303	1.096117
35	8	0	-1.553412	-1.047983	-0.601775
36	1	0	0.973516	-0.856981	-1.831974
37	6	0	-3.951641	-0.562960	-1.426441
38	9	0	-5.035793	0.188599	-1.247826
39	9	0	-3.495502	-0.354782	-2.661967
40	9	0	-4.298818	-1.842598	-1.316146

Optimized Cartesian coordinates for ts-in45

Center Number	Atomic Number	Atomic Type	Coordinates (Angstroms)		
			X	Y	Z
1	6	0	2.236787	0.910934	-0.294755
2	6	0	1.541379	1.016069	-1.640574
3	6	0	0.438478	0.147422	-1.744001
4	6	0	0.311331	-0.544113	-0.484141
5	8	0	3.118950	-0.550823	-0.535862
6	8	0	2.913533	1.781174	0.205478
7	6	0	1.881307	1.872261	-2.674582
8	6	0	1.144241	1.794316	-3.855252
9	6	0	0.069691	0.904892	-3.979650
10	6	0	-0.297757	0.074448	-2.927661
11	1	0	2.714995	2.558370	-2.563697
12	1	0	1.411908	2.423894	-4.698017

13	1	0	-0.490430	0.872240	-4.908379
14	1	0	-1.157491	-0.582910	-3.009329
15	6	0	0.915850	0.218477	0.597046
16	8	0	1.176613	-0.700339	1.629492
17	6	0	0.241480	1.452471	1.171103
18	1	0	-0.653611	1.165987	1.728092
19	1	0	0.959168	1.944383	1.832248
20	1	0	-0.027145	2.144025	0.370073
21	6	0	0.713859	-1.891666	1.242499
22	6	0	0.132147	-1.859117	-0.055271
23	6	0	0.829628	-3.070704	1.980890
24	6	0	-0.337106	-3.058106	-0.649589
25	1	0	3.314132	-1.223826	0.297619
26	6	0	0.343249	-4.210951	1.379008
27	1	0	1.341438	-3.083726	2.935068
28	6	0	-0.248154	-4.209414	0.084438
29	1	0	-0.746953	-3.051488	-1.653697
30	1	0	0.451808	-5.157940	1.897679
31	1	0	-0.590751	-5.149205	-0.333412
32	16	0	3.662845	-3.562457	0.568435
33	8	0	2.779343	-3.628573	-0.591676
34	8	0	3.610556	-4.636762	1.546106
35	8	0	3.662207	-2.190659	1.206381
36	1	0	3.997794	-0.236637	-0.812850
37	6	0	5.351607	-3.606659	-0.141726
38	9	0	5.522154	-4.694753	-0.882667
39	9	0	5.528661	-2.530849	-0.920987
40	9	0	6.272241	-3.586919	0.813693

Optimized Cartesian coordinates for ts-i12

Center Number	Atomic Number	Atomic Type	Coordinates (Angstroms)		
			X	Y	Z
1	6	0	3.477529	-0.144503	-2.078859
2	6	0	3.803505	-0.733996	-0.847074
3	6	0	2.819662	-1.149675	0.042423
4	6	0	1.485901	-0.962645	-0.320318
5	6	0	1.166971	-0.403289	-1.551424
6	6	0	2.149809	0.022153	-2.444749
7	6	0	0.251589	-1.311797	0.481597
8	6	0	-0.300060	-0.436401	-1.756495
9	8	0	-0.906357	-0.010542	-2.715478
10	8	0	0.256500	-2.283250	1.300535
11	1	0	4.272122	0.177809	-2.745918
12	1	0	4.850500	-0.860459	-0.583027
13	1	0	3.067607	-1.586317	1.007227
14	1	0	1.863123	0.458783	-3.397194
15	6	0	-0.923421	-1.219617	-0.576880
16	6	0	-1.140496	-2.653193	-1.076997
17	1	0	-1.533587	-3.264744	-0.260678
18	1	0	-1.821625	-2.667653	-1.933612
19	1	0	-0.184722	-3.087343	-1.384856
20	6	0	-2.205015	-0.540485	-0.142500
21	6	0	-3.472427	-1.073735	-0.364413
22	6	0	-2.108325	0.753437	0.404321
23	6	0	-4.621979	-0.340909	-0.066566
24	1	0	-3.575503	-2.068471	-0.784986

25	6	0	-3.255879	1.490520	0.681117
26	6	0	-4.517164	0.947430	0.443583
27	1	0	-5.600037	-0.779483	-0.245581
28	1	0	-3.147710	2.486554	1.102347
29	1	0	-5.410196	1.524356	0.667765
30	6	0	-0.750647	1.248776	0.721213
31	6	0	-0.236186	2.397384	0.209475
32	6	0	0.038316	0.337773	1.525420
33	6	0	1.116784	2.852457	0.550676
34	1	0	-0.809581	3.018526	-0.474210
35	6	0	1.339780	0.820727	1.935478
36	1	0	-0.524542	-0.226877	2.265031
37	6	0	1.866824	1.970517	1.453224
38	1	0	1.929475	0.179006	2.589287
39	1	0	2.870302	2.294181	1.715527
40	8	0	1.585394	3.906809	0.113297
41	1	0	1.667990	-1.731487	3.834774
42	8	0	2.177835	-2.226576	3.180481
43	1	0	1.518739	-2.343739	2.445033

Optimized Cartesian coordinates for ts-II3

Center Number	Atomic Number	Atomic Type	Coordinates (Angstroms)		
			X	Y	Z
1	6	0	-2.507098	4.812700	-3.307177
2	6	0	-2.767721	3.551677	-3.854842
3	6	0	-2.264478	2.387614	-3.273065
4	6	0	-1.480060	2.508714	-2.132622
5	6	0	-1.203466	3.770880	-1.607956
6	6	0	-1.715910	4.935079	-2.169893
7	6	0	-0.912167	1.429217	-1.203465
8	6	0	-0.279462	3.625714	-0.451584
9	8	0	0.016394	4.473919	0.357746
10	8	0	-1.926911	1.064664	-0.271683
11	1	0	-2.917339	5.698002	-3.782669
12	1	0	-3.375251	3.479490	-4.752120
13	1	0	-2.472568	1.417610	-3.714193
14	1	0	-1.482646	5.901167	-1.732150
15	6	0	0.260769	2.183472	-0.500857
16	6	0	0.622178	1.640601	0.876291
17	1	0	1.066196	0.644440	0.787917
18	1	0	1.344973	2.308862	1.351635
19	1	0	-0.264906	1.571949	1.509390
20	6	0	1.491513	2.232459	-1.414212
21	6	0	2.431975	3.254636	-1.259990
22	6	0	1.722008	1.241045	-2.382453
23	6	0	3.558840	3.321142	-2.071598
24	1	0	2.270156	4.012379	-0.498370
25	6	0	2.847383	1.327757	-3.208358
26	6	0	3.760672	2.361399	-3.061123
27	1	0	4.272096	4.128446	-1.938524
28	1	0	2.991398	0.577030	-3.980344
29	1	0	4.626979	2.417380	-3.712623
30	6	0	0.809802	0.087644	-2.492513
31	6	0	1.233994	-1.153410	-2.893531
32	6	0	-0.486716	0.141520	-1.844516
33	6	0	0.266088	-2.112071	-2.415392

34	1	0	2.288526	-1.402384	-2.933620
35	6	0	-1.506496	-0.730841	-2.407877
36	1	0	0.010579	-1.206359	-0.875777
37	6	0	-1.126662	-1.969141	-2.811132
38	1	0	-2.552954	-0.466901	-2.285202
39	1	0	-1.807594	-2.804981	-2.911954
40	8	0	0.416763	-2.413181	-1.167149
41	1	0	-2.399640	1.869687	-0.009278

Optimized Cartesian coordinates for ts-III

Center Number	Atomic Number	Atomic Type	Coordinates (Angstroms)		
			X	Y	Z
1	6	0	-3.577950	-1.821164	-1.797472
2	6	0	-2.383122	-2.493203	-2.095368
3	6	0	-1.220570	-2.216010	-1.385178
4	6	0	-1.301291	-1.261373	-0.367786
5	6	0	-2.502686	-0.592709	-0.068900
6	6	0	-3.651403	-0.855795	-0.787599
7	6	0	-0.278982	-0.699595	0.465822
8	6	0	-2.256325	0.347758	1.102344
9	8	0	-3.075826	1.159525	1.524500
10	8	0	-1.842373	-1.090672	2.171098
11	1	0	-4.466719	-2.057077	-2.376305
12	1	0	-2.367256	-3.222536	-2.898587
13	1	0	-0.279220	-2.702843	-1.624891
14	1	0	-4.571637	-0.327852	-0.557690
15	6	0	-0.709190	0.589470	1.068798
16	6	0	-0.154663	0.932001	2.459474
17	1	0	0.913688	1.163215	2.420840
18	1	0	-0.694398	1.820680	2.799957
19	1	0	-0.347283	0.114607	3.151261
20	6	0	-0.178702	1.644990	0.106231
21	6	0	-0.899758	2.794602	-0.189101
22	6	0	1.136422	1.472513	-0.373763
23	6	0	-0.327637	3.779023	-0.993441
24	1	0	-1.902918	2.895113	0.216527
25	6	0	1.689971	2.467613	-1.181794
26	6	0	0.962803	3.614324	-1.488695
27	1	0	-0.894578	4.671520	-1.239766
28	1	0	2.684860	2.343052	-1.598625
29	1	0	1.404779	4.375274	-2.124153
30	6	0	1.874318	0.219391	-0.044919
31	6	0	3.245528	0.086314	-0.215490
32	6	0	1.138881	-0.935251	0.355248
33	6	0	3.877134	-1.142064	0.003184
34	1	0	3.864957	0.925705	-0.511101
35	6	0	1.768943	-2.168424	0.516724
36	1	0	5.552560	-2.060996	0.020075
37	6	0	3.142706	-2.275897	0.363049
38	1	0	1.178126	-3.029043	0.815841
39	1	0	3.645275	-3.225285	0.526684
40	8	0	5.218760	-1.171050	-0.163251
41	1	0	-2.493577	-1.792493	2.008774

Optimized Cartesian coordinates for ts-III4

Center Number	Atomic Number	Atomic Type	Coordinates (Angstroms)		
			X	Y	Z
1	6	0	-3.716634	4.050979	-3.056807
2	6	0	-3.879454	2.884226	-3.851999
3	6	0	-2.924866	1.900028	-3.853998
4	6	0	-1.784672	2.061266	-3.016694
5	6	0	-1.599203	3.264560	-2.292320
6	6	0	-2.583164	4.258167	-2.300859
7	6	0	-0.657077	1.235415	-2.793492
8	6	0	-0.173581	3.392022	-1.766387
9	8	0	0.447856	4.172351	-2.599909
10	8	0	-0.140362	3.855033	-0.407763
11	1	0	-4.499147	4.805159	-3.076996
12	1	0	-4.760187	2.790222	-4.478726
13	1	0	-3.032506	1.044494	-4.510994
14	1	0	-2.429399	5.169393	-1.731900
15	6	0	0.264556	1.850533	-1.793553
16	6	0	-0.064607	1.165508	-0.434495
17	1	0	0.109355	0.085462	-0.479779
18	1	0	0.578396	1.613148	0.324522
19	1	0	-1.105424	1.359916	-0.159139
20	6	0	1.707429	1.614617	-2.119657
21	6	0	2.676981	2.476795	-1.606040
22	6	0	2.091385	0.507658	-2.893651
23	6	0	4.019799	2.258462	-1.878206
24	1	0	2.352574	3.331449	-1.023525
25	6	0	3.452704	0.307385	-3.171133
26	6	0	4.408507	1.174295	-2.668027
27	1	0	4.767336	2.943948	-1.491007
28	1	0	3.768007	-0.517900	-3.800986
29	1	0	5.457221	1.011472	-2.895652
30	6	0	1.053316	-0.418183	-3.384825
31	6	0	1.378566	-1.665335	-3.912139
32	6	0	-0.324236	-0.034847	-3.352731
33	6	0	0.391534	-2.524833	-4.386905
34	1	0	2.402409	-2.016849	-3.948723
35	6	0	-1.304801	-0.931721	-3.826029
36	1	0	0.034486	-4.225502	-5.179152
37	6	0	-0.965033	-2.165038	-4.333331
38	1	0	-2.351805	-0.673328	-3.722010
39	1	0	-1.730322	-2.861477	-4.665248
40	8	0	0.797980	-3.714751	-4.872780
41	1	0	0.257468	4.731641	-0.534188